Journal of Hazardous Materials 432 (2022) 128657

Contents lists available at ScienceDirect

Journal of Hazardous Materials

journal homepage: www.elsevier.com/locate/jhazmat

Efficient removal of arsenic from aqueous solution by continuous adsorption onto iron-coated cork granulates

Mariko A. Carneiro [a,b], Ariana M.A. Pintor [a,b,*], Rui A.R. Boaventura [a,b], Cidália M.S. Botelho [a,b]

[a] LSRE-LCM - Laboratory of Separation and Reaction Engineering – Laboratory of Catalysis and Materials, Faculty of Engineering, University of Porto, Rua Dr. Roberto Frias, 4200-465 Porto, Portugal
[b] ALiCE - Associate Laboratory in Chemical Engineering, Faculty of Engineering, University of Porto, Rua Dr. Roberto Frias, 4200-465 Porto, Portugal

HIGHLIGHTS

- Iron-coated cork granulates (ICG) efficiently removed arsenic in continuous mode.
- Flow rate and bed height statistically influenced ICG fixed-bed column performance.
- A pH increase reduced As(V) adsorption and increased As(III) adsorption.
- Adsorption capacities of 4.2 mg As(V) g^{-1}, and 1.8 mg As(III) g^{-1} were achieved.
- The thermodynamic study has proven the process to be spontaneous and endothermic.

GRAPHICAL ABSTRACT

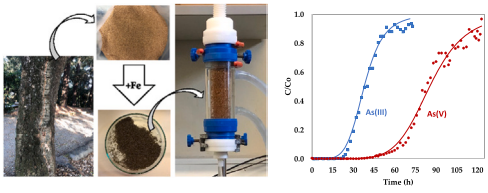

ARTICLE INFO

Editor: Dr. Rinklebe Jörg

Keywords:
Fixed-bed adsorption column
Modified biosorbent
Breakthrough curve
Factorial design
Thermodynamics

ABSTRACT

The search for low-cost technologies for arsenic removal from water is in high demand due to its human toxicity, even at low concentrations. Adsorption can be a cost-effective water treatment technique if applied with inexpensive materials. Arsenic continuous removal by adsorption onto an alternative modified biosorbent, iron-coated cork granulates (ICG), was investigated in this work. Results showed that most experimental parameters of breakthrough curves (BTC) depend on flow rate, bed height, pH, and initial arsenic concentration. The temperature did not significantly affect arsenate removal in continuous mode; however, the adsorption capacity was affected in batch mode. The thermodynamic parameters suggest that the adsorption process is spontaneous and endothermic. The maximum adsorption capacity of ICG for As(V) removal at pH 3 was 4.2 ± 0.3 mg g^{-1}, calculated by Yan model fit ($R^2 = 0.981$), and for As(III) at pH 9 was 1.6 ± 0.2 mg g^{-1} ($R^2 = 0.994$). ICG were able to treat As(V) from 100 μg L^{-1} to under 10 μg L^{-1} and 50 μg L^{-1} for 895 and 1633 bed volumes, and As(III) for 569 and 861 bed volumes, respectively, both at pH 7. The application of ICG in arsenic oxyanions remediation was found to be effective under various conditions.

* Corresponding author at: LSRE-LCM - Laboratory of Separation and Reaction Engineering – Laboratory of Catalysis and Materials, Faculty of Engineering, University of Porto, Rua Dr. Roberto Frias, 4200-465 Porto, Portugal.
E-mail address: ampintor@fe.up.pt (A.M.A. Pintor).

https://doi.org/10.1016/j.jhazmat.2022.128657
Received 20 December 2021; Received in revised form 7 February 2022; Accepted 7 March 2022
Available online 9 March 2022

Nomenclature

ANOVA	Analysis of variance
ATP	Adenosine triphosphate
BTC	breakthrough curve
DoE	Design of experiments
FAAS	flame atomic absorption spectrometry
GFAAS	graphite furnace atomic absorption spectrometry
ICG	iron-coated cork granulates
SE	standard error
S/L	solid/liquid ratio

List of symbols

a_{ya}	Yan model empirical parameter
BV_b	bed volume at breakthrough
BV_s	bed volume at saturation
C_f	final concentration of the adsorbate (mg L^{-1})
C_i	initial concentration of the adsorbate (mg L^{-1})
K_o	Standard equilibrium constant
K_F	Freundlich constant ($mg^{(1-1/n)}$ $L^{1/n}$ g^{-1})
K_L	Langmuir constant (L mg^{-1})
K_{YN}	kinetic constant of Yoon-Nelson model (min^{-1})
m	mass of adsorbent (g)
M	mass of adsorbent in the column (g)
MTZ	mass transfer zone length (cm)
n	dimensionless parameter related to adsorbent-adsorbate affinity
p	probability of observing variation in results due to random factors
q	adsorption capacity (mg g^{-1})
q_b	adsorption capacity at breakthrough (mg g^{-1})
q_e	adsorption capacity at equilibrium (mg g^{-1})
q_{TH}	Thomas model predicted adsorption capacity (mg g^{-1})
q_s	adsorption capacity at saturation point (mg g^{-1})
Q_{ya}	Yan model predicted adsorption capacity (mg g^{-1})
r^2	correlation coefficient
R	gas constant of 8.314×10^{-3} kJ/(mol K).
t	time (h)
t_b	time of breakthrough (h)
t_{exp} 50%	time required to achieve 50% saturation (min)
t_s	saturation time
t_{YN} 50%	Yoon-Nelson predicted time required to achieve 50% saturation (min)
T	temperature (°C)
T_K	temperature (K)
V	solution volume (L)
V_b	breakthrough volume (L)
V_s	saturation volume (L)
y_b	arsenic removal efficiency at breakthrough (%)
y_s	arsenic removal efficiency at saturation (%)
α	significance level
ΔG^0	standard Gibbs free energy change
ΔH^0	enthalpy change
ΔS^0	entropy change

1. Introduction

Arsenic (As) is a pnictogenic element, chemically classified as a metalloid, which shares the same periodic table group with antimony (Sb) and phosphorus (P). Most common inorganic species contain either pentavalent or trivalent As, being the last one much more noxious to humans. “Arsenates” are by definition compounds of As(V) and oxygen, and “arsenite” compounds of As(III) and oxygen. Arsenate can act as a potential oxidative phosphorylation inhibitor, and arsenite can bind with reactive sulfur atoms present in many enzymes (Lim et al., 2014). The consumption of these forms of As is a serious concern due to their ability to interfere in vital processes in the human body, such as ATP production and respiration (Lim et al., 2014).

Arsenic belongs to group 1 from carcinogen agents, and its major human exposure routes are through direct drinking of contaminated water and ingestion of food grown or cooked by polluted water (Sharma et al., 2014; Natasha et al., 2021). The guideline value established for arsenic in drinking water is 10 μg L^{-1} (World Health Organization, 2011; European Commission, 2008). However, some developing countries still use less safe guidelines such as 30 and 50 μg L^{-1}.

Arsenic poisoning can lead to serious human health effects even at low concentrations. Approximately 230 million people worldwide are affected by arsenic contamination in 108 countries, spread in all six continents, but mainly in Southeast Asia (Shaji et al., 2021), where water infrastructure is deficient in attaining safe limits, and the solution primarily depends on affordable treatment technologies.

Conventional processes such as precipitation, coagulation and membrane separation for advanced water treatment are disadvantageous either due to high operational cost (Brion-Roby et al., 2018) or formation of toxic sludge (Ungureanu et al., 2017). Adsorption is a simple and efficient process for water remediation, and several studies have explored the removal of arsenic (Carneiro et al., 2021; Hao et al., 2018; Asere et al., 2019; Lata and Samadder, 2016; Dias and Fontes, 2020; Mondal and Garg, 2017) and other pollutants. Biosorbents and other more cost-effective materials are replacing traditional adsorbents such as alumina and activated carbon.

Cork materials are organic and renewable sources of biosorbents, originated from the bark of tree species *Quercus suber* L. Silva et al. (2005). Cork granulates are byproducts from the industrial grinding process (Pintor et al., 2012), which gained attention in water remediation due to their physical and chemical stability. Their application in adsorption became even more relevant after modification to iron-coated cork granulates (ICG) (Pintor et al., 2018). Studies in batch mode have proved ICG to effectively adsorb arsenic, antimony, and phosphorus (Pintor et al., 2018, 2020b; Bacelo et al., 2020).

For industrial and commercial purposes, the adsorption treatment in continuous mode, more specifically in a fixed-bed column, is preferable (Patel, 2019). Previous studies using other adsorbents reported that fixed-bed columns for arsenic treatment could be affected by temperature, pH, flow rate, adsorbent quantity (bed height), hydraulic retention time, initial concentration of adsorbate, and the presence of other chemical components (Carneiro et al., 2021), such as competitive ions (sulfate, phosphate, bicarbonate, nitrate, chloride), and natural organic matter (Sosa et al., 2020).

This work aimed to investigate arsenate removal from aqueous solution by ICG in fixed-bed adsorption columns. The effects of flow rate, temperature, bed height (adsorbent amount), pH and arsenic initial concentration on breakthrough curves parameters were evaluated in order to explore and optimize a laboratory-scale adsorption column. Batch mode experiments were also carried out for thermodynamic studies.

2. Materials and methods

2.1. Materials

The raw cork granulates (RCG) were provided by Corticeira Amorim, S.G.P.S., with a particle size of 0.5–1.0 mm. The iron-coated cork

granulates (ICG) were produced as described in a previous study (Pintor et al., 2018) and applied in other works (Pintor et al., 2018, 2021, 2020a, 2020b). The iron content was on average 25 ± 2 mg g^{-1}.

Arsenic inlet solutions were prepared by diluting, in distilled water, a standard solution of 995 ± 81 mg As(V) L^{-1}, originated from HAs-$Na_2O_4{\cdot}7H_2O$ (Sigma-Aldrich; analytical grade) in 2% HCl, and a standard solution of 939 ± 35 mg As(III) L^{-1}, originated from As_2O_3 (Acros Organics; 99.5%) in 4% HNO_3.

The pH was regulated using 0.1 M, 1 M and 10 M NaOH or HNO_3 solutions.

2.2. Analytical methods

The concentration of arsenic in aqueous solution, both in batch and continuous study, was determined by flame atomic absorption spectrometry (FAAS) for concentrations in the range 5–50 mg L^{-1} and graphite furnace atomic absorption spectrometry (GFAAS) for concentrations ranging from 6.7 to 50 µg L^{-1}. Total dissolved iron was measured by FAAS, in the range 0.25–5 mg L^{-1}.

The equipments for FAAS and GFAAS were a GBC 932 Plus spectrometer and a GBC GF3000-SensAA Dual spectrometer, respectively. Detailed information on analytical conditions is provided in Supplementary Materials.

2.3. Evaluation of temperature effect in batch operation mode and thermodynamic studies

2.3.1. Arsenate adsorption

Despite the fact that recent studies have investigated As(V) adsorption by ICG in batch mode (Pintor et al., 2020b, 2021), the temperature influence had not yet been assessed. However, this is an important parameter for thermodynamic analysis and the design of a fixed-bed system. The effect of temperature was assessed in As(V) adsorption onto iron-coated cork granulates in batch operation mode by the determination of isotherms at temperatures of 10.0 ± 0.5 °C, 20.0 ± 0.5 °C and 30.0 ± 0.5 °C. As(V) solutions at initial concentrations of 1, 5, 10, 15, 25 and 40 mg L^{-1} were adjusted to pH 3.0 with NaOH and HNO_3. The pH choice was made considering the earlier published results from As(V) adsorption by ICG in batch mode, in which the optimum pH value was observed to be 3.0 (Pintor et al., 2018). A volume of 45 mL of As(V) solution was put in contact with the adsorbents at a solid/liquid ratio of 2.5 g L^{-1}, over 48 h (Pintor et al., 2018), in a rotating shaker (20 rpm). Then, the samples were filtered through cellulose acetate membrane filters (0.45 µm porosity), followed by As quantification. The experiments were done in duplicate (n = 2).

The adsorbed amount of As(V) per mass of iron-coated cork granulates (q) was calculated according to Eq. (1).

$$q = \frac{V \quad (C_i - C_f)}{m} \tag{1}$$

Where V is the solution volume (L), C_i and C_f are the initial and final concentrations of the adsorbate (mg L^{-1}), respectively, and m is the mass of adsorbent (g).

The Langmuir (Langmuir, 1918) and Freundlich (Freundlich, 1907) models in their linearized form (Eq. (2) and Eq. (3), respectively) were fitted to the experimental data to generate the equilibrium isotherms. The models relate the adsorption capacity of As(V) at equilibrium q_e (mg g^{-1}) with the equilibrium concentration C_e (mg L^{-1}).

$$\frac{C_e}{q_e} = \frac{1}{K_L \quad q_{max}} + \frac{C_e}{q_{max}} \tag{2}$$

$$logq_e = logK_F + \frac{1}{n} logC_e \tag{3}$$

Where K_L is the Langmuir constant (L mg^{-1}), K_F is the Freundlich constant ($mg^{(1-1/n)}$ $L^{1/n}$ g^{-1}), q_{max} is the maximum adsorption capacity (mg g^{-1}), and n is a dimensionless parameter related to adsorbent-adsorbate affinity.

The iron content in the final solution was measured to assess the metal leaching from the adsorbent at different temperatures.

2.3.2. Thermodynamic studies

The standard Gibbs free energy change (ΔG^0), entropy change (ΔS^0), and enthalpy change (ΔH^0), were estimated to evaluate the adsorption process, using the following equations:

$$\Delta G^0 = \quad -RTLnKo \tag{4}$$

$$\Delta G^0 = \Delta H^0 - T_K \Delta S^0 \tag{5}$$

The combination of Eq. (4) and Eq. (5) leads to:

$$Ln \quad K_o = \quad \frac{\Delta S^0}{R} - \frac{\Delta H^0}{RT_K} \tag{6}$$

Where T_K is the temperature in Kelvin (K), K_o is the standard equilibrium constant, and R is the gas constant of 8.314×10^{-3} kJ mol^{-1} K^{-1}.

2.4. Fixed-bed column experiments

Arsenic continuous adsorption assays were taken in a fixed-bed column operating in downward flow due to the low density of the adsorbent. The lab-scale continuous adsorption system consisted of an influent reservoir of 50 L; a glass column (*Chromaflex*®) with 2.5 cm internal diameter and 15 cm of maximum height; an outlet reservoir of 30 L; a thermostatic bath for temperature control (DIGIT-COOL, J.P. SELECTA), a peristaltic pump for flow rate regulation (VWR); and an automatic sampler (GILSON, FC-203B). Fig. 1 presents a diagram of the lab-scale experimental structure.

Before each experiment, the adsorbent was hydrated in distilled water and put into vacuum to remove the air trapped into the pores. The column was packed with the adsorbent and fed by distilled water for 2 h, at similar flow rate of the following experiment.

2.4.1. Optimization of fixed-bed column

A 2-level 3-factor (2^3) design of experiments (DoE) was conducted to investigate the effect of each operational parameter, described in item 2.4.2. Three factors were selected, each with two levels: flow rate of 5 mL min^{-1} (−1) and 10 mL min^{-1} (+1); bed height of 6 cm (−1) and 12 cm (+1); and temperature of 10 °C (−1) and 30 °C (+1). The amount of adsorbent corresponding to bed heights of 6 and 12 cm was 3 and 6 g, respectively.

The flow rate and bed height levels were based on other studies of adsorption column for arsenic removal (Saha and Sarkar, 2016; Brion-Roby et al., 2018; Nguyen et al., 2020; Dhoble et al., 2017; Chen and Chung, 2006; Sarkar et al., 2010). Moreover, the quantity of 3–6 g was considered a feasible amount of adsorbent to be produced in lab-scale. The temperature levels were defined regarding the range of groundwater temperature in arsenic affected countries.

In total, eight runs were performed in the fixed-bed column, according to Table 1. Each run was repeated once (n = 1).

The bed volume (BV) for the column packed up to 6 and 12 cm was 29 and 59 mL, respectively.

The iron leached from the adsorbent to the aqueous stream was monitored throughout the experiment, every two hours.

The results of the DoE were analyzed using the software *Minitab 19*, including the ANOVA for each characterization parameter.

2.4.2. Analysis of breakthrough curves (BTC)

The fixed-bed column performance was evaluated by breakthrough curves (BTC), which consisted in the plot of the ratio of effluent concentration C (mg L^{-1}) to influent concentration C_o (mg L^{-1}) versus flow time t (min). Breakthrough time (t_b) was fixed as the moment when the

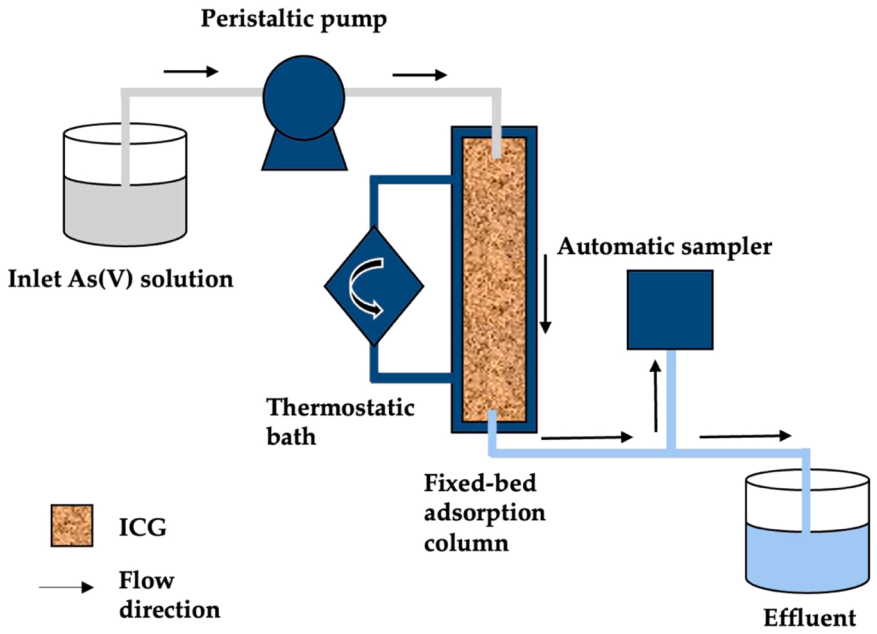

Fig. 1. Schematic diagram of the lab-scale adsorption system of fixed-bed column.

Table 1
Levels of each factor for each fixed-bed column run of the 2^3 factorial design.

Run #	Flow rate – Q (mL min^{-1})	Bed height – Z (cm)	Temperature – T (°C)
1	5	6	30
2	10	6	10
3	5	12	10
4	10	12	30
5	10	6	30
6	5	12	30
7	5	6	10
8	10	12	10

effluent concentration reached 10 μg L^{-1}. Saturation time (t_s) was fixed as the moment when the effluent concentration achieved approximately 90% of the initial concentration. Other experimental breakthrough parameters calculated in this work were: adsorption capacity at breakthrough (q_b); adsorption capacity at the saturation point (q_s); bed volume treated at breakthrough (BV_b); bed volume treated at the saturation point (BV_s); breakthrough volume (V_b) and the saturation volume (V_s) (Ungureanu et al., 2017); arsenic removal at breakthrough (y_b), and arsenic removal at saturation (y_s); the mass transfer zone of the column (MTZ); and, finally, the MTZ/Bed height ratio.

To determine the adsorption capacity, the amount of arsenic loaded in the column $m_{in,t}$ at time t and the amount of unadsorbed arsenic $m_{out,t}$ at time t were calculated (Chatterjee and Schiewer, 2011). The amount of mass (g) loaded can be expressed in terms of initial concentration C_o (mg L^{-1}), flow rate Q (L min^{-1}) and time t (min). Then, the amount of arsenic adsorbed in the column $m_{ad,t}$ at time t was calculated as the difference between $m_{in,t}$ and $m_{out,t}$:

$$m_{ad,t} = m_{in,t} - m_{out,t} = \quad C_oQt - C_oQt\int_o^{t_b}\left(\frac{C}{Co}\right)dt \tag{7}$$

In this way, the adsorption capacity at breakthrough (q_b) was determined as the total mass of arsenic adsorbed at breakthrough $m_{ad,t}$ divided by the mass of adsorbent in the reactor, M (g):

$$q_b = \frac{m_{ad,t_b}}{M} = \frac{C_oQ\int_o^{t_b}\left(1-\frac{C}{Co}\right)dt}{M} \tag{8}$$

Similarly, the adsorption capacity at saturation (q_s) was determined as:

$$q_s = \frac{m_{ads,t_s}}{M} = \frac{C_oQ\int_o^{t_s}\left(1-\frac{C}{Co}\right)dt}{M} \tag{9}$$

The arsenic removal (y) is the percentage of arsenic mass retained in the adsorbent at a certain time. It was calculated for t_b and t_s as follows:

$$\text{yb} = 1 - \frac{m_{out,t_b}}{m_{in,t_b}} \times 100 \tag{10}$$

$$\text{ys} = 1 - \frac{m_{out,t_s}}{m_{in,t_s}} \times 100 \tag{11}$$

The mass transfer zone length of the column (MTZ) (cm) was determined by Eq. (12), where H is the packed bed height (Ungureanu et al., 2017). It is an important parameter to consider for the scale-up of the column, related to the efficiency of the adsorption process (Verduzco-Navarro et al., 2020).

$$MTZ = H \times \quad \frac{t_s - \quad t_b}{t_s} \tag{12}$$

2.4.3. Fixed-bed theoretical models

Three models were applied, using nonlinear regression, to describe the experimental breakthrough curves. The fittings were carried out using *Minitab 19* and *Curve Expert Pro 2.7* softwares.

2.4.3.1. Thomas model (TH). Thomas model (Thomas, 1944) is a common model for adsorption-desorption without axial dispersion in a fixed-bed column that assumes Langmuir kinetics, expressed by the equation:

$$\frac{C}{C_o} = \frac{1}{1+\exp(k_{TH}(q_{TH}m/Q - \quad C_ot))} \tag{13}$$

Where k_{TH} is the Thomas model constant rate (L min^{-1} mg^{-1}), q_{TH} is the theoretical saturation adsorption capacity (mg g^{-1}), m is the mass of adsorbent in the column (g), Q is the flow rate (L min^{-1}), C_o is the initial adsorbate concentration (mg L^{-1}), t is flow time (min), and C is the concentration of adsorbate at time t (mg L^{-1}).

2.4.3.2. Yoon-Nelson (YN). The Yoon-Nelson model (Yoon and Nelson,

1984) equation is:

$$\frac{C}{C_o} = \frac{\exp(k_{YN} * t - \tau_{YN} * k_{YN})}{1 + \exp(k_{YN} * t - \tau_{YN} * k_{YN})} \quad (14)$$

Where k_{YN} is the Yoon-Nelson constant rate (min $^{-1}$), τ_{YN} is the predicted time required for 50% of adsorbate breakthrough (C/C$_o$ = 0.5) (min), C_o is the initial adsorbate concentration (mg L^{-1}), t is flow time (min), and C is the concentration of adsorbate at time t (mg L^{-1}).

2.4.3.3. Yan model. The Yan model (Yan et al., 2001) is an empirical model developed to minimize the errors from the Thomas model, represented by the equation:

$$\frac{C}{C_o} = 1 - \frac{1}{1 + \left(\frac{C_o Q}{q_{Ya} * m} * t\right)^{a_{Ya}}} \quad (15)$$

Where a_{Ya} is an empirical parameter, q_{Ya} is the theoretical saturation adsorption capacity (mg g^{-1}), m is the mass of adsorbent in the column (g), Q is the flow rate (L min^{-1}), C_o is the initial adsorbate concentration (mg L^{-1}), t is flow time (min), and C is the concentration of adsorbate at time t (mg L^{-1}).

2.4.4. Effect of temperature

The influence of temperature on breakthrough curves of As(V) adsorption was analyzed for the range of 10–30 °C. The column operating parameters were: bed height = 12 cm, flow rate = 5 mL min $^{-1}$, initial concentration = 1 mg L^{-1}, and pH = 3.0. These correspond to the optimized configuration found from the results of previous experiments (item 2.4.1). Each run was repeated once (n = 1).

2.4.5. Effect of pH

The pH effect on breakthrough curves was evaluated adjusting pH to values of 3.0, 7.0 and 9.0 for As(V) and 7.0 and 9.0 for As(III). The studies were conducted at a flow rate of 5 mL min $^{-1}$, a bed height of 12 cm, and an initial concentration of 1 mg L^{-1}, at 20.0 ± 0.3 °C. These are the optimal values previously found for those parameters (item 2.4.1). Each run was repeated once (n = 1).

2.4.6. Effect of initial concentration

The effect of the initial influent concentration in continuous arsenic adsorption was investigated using arsenic solutions of 0.1 and 1.0 mg L^{-1} for each oxidation state. The studies were conducted at a flow rate of 5 mL min $^{-1}$, 12 cm bed height, pH 7, and a temperature of 20.0 ± 0.3 °C. Those parameters were obtained from previous optimization experiments (item 2.4.1). Each run was repeated once (n = 1).

3. Results and discussion

3.1. Evaluation of temperature effect on batch mode operation and thermodynamic studies

3.1.1. Arsenate adsorption

Equilibrium isotherms of arsenate adsorption onto iron-coated cork granulates were obtained at different temperatures. The Langmuir and Freundlich linearized curves for each temperature are displayed in Fig S.2 (Supplementary Materials). The experimental data and the corresponding Langmuir curves can be found in Table S.1 and Fig. 2, respectively.

The Langmuir isotherm fits better the equilibrium data (Table S.1), with correlation coefficients above 0.98. Even though showing a worse fit, Freundlich still presented a good correlation ($r^2 > 0.92$). Earlier isotherm equilibrium studies of As(V) conducted with ICG at 20 °C at similar conditions (Pintor et al., 2018) led to similar results, though *Qmax* was lower: 6.2 ± 0.2 mg g^{-1} in this study and 3.8 ± 0.2 mg g^{-1} in the cited study. This difference can be explained by the variation in the iron content of ICG, the heterogeneity of the material, and particle size, which was previously 0.8–1.0 mm and now 0.5–1.0 mm.

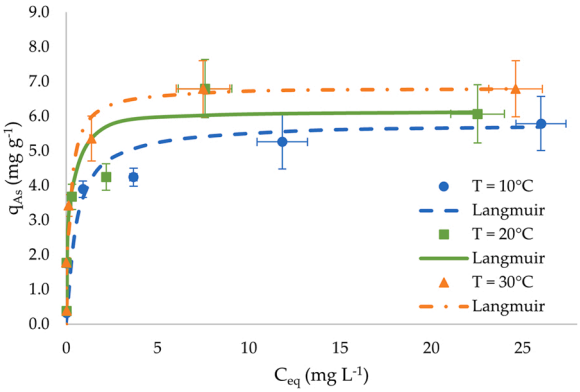

Fig. 2. Langmuir adsorption isotherms of As(V) on ICG (pH 3.0; S/L ratio = 2.5 g L^{-1}; contact time = 48 h) for temperatures of 10, 20 and 30 °C (Error bars: maximum absolute deviation).

Temperature affects the As(V) adsorption capacity of ICG, indicated by the Langmuir maximum adsorption capacity (*Qmax*) and Freundlich constant (K_F). When plotting both parameters versus temperature, a good direct proportionality correlation ($R^2 > 0.97$) was observed between Qmax or K_F and temperature, as shown in Fig. S.1.

Analogous temperature effect on arsenic adsorption was noticed for other iron-modified biosorbents, such as iron oxide impregnated carbon from Tamarind hull (IOITHC) (Maiti et al., 2010), iron modified root powder (Lin et al., 2018), iron-loaded activated carbon using waste biomass (Liu et al., 2010); and other adsorbents such as magnetite nanoparticles (Shipley et al., 2009). A possible cause for the effect is the increase in the kinetic activity in the solution, causing an increase in the rate of arsenate contact with the adsorbent. Different results, though, were observed for arsenic removal by iron-impregnated granular activated carbon (GAC-Fe), in which a variation of temperature from 30 to 60 °C did not affect the results (Mondal et al., 2007). The same study considered that arsenic forms more stable bonds with the iron oxides active sites from GAC-Fe, in comparison to GAC, whose removal percentage decreased with the temperature increase. The process proved to be exothermic.

In the equilibrium experiments of As(V), the iron concentration in the equilibrium solution was measured to monitor the iron leached from ICG. The total dissolved iron in equilibrium at 10, 20 and 30 °C varied from 0.5 ± 0.2–0.9 ± 0.2 mg L^{-1}, 0.8 ± 0.2–1.7 ± 0.2 mg L^{-1}, and 1.3 ± 0.2–2.6 ± 0.2 mg L^{-1}, respectively. The iron leached into the solution at equilibrium exceeded the guideline concentration in drinking water of 0.3 mg L^{-1} (ppm) (World Health Organization, 2011) and increased with temperature, which can be a possible disadvantage for the application of ICG on effluents with high temperatures. However, the equilibrium studies were conducted at pH 3, and the acid solution is more favorable for iron leaching than natural waters, whose pH is closer to neutrality.

3.1.2. Thermodynamic studies

The results from the last Section 3.1.1 indicate endothermic adsorption of As(V) onto ICG since adsorption capacity increased with temperature. To better understand that behavior, thermodynamic studies were conducted.

The values of K_o were obtained from the Langmuir model parameter K_L (L mg^{-1}) (Table S.1). K_o was transformed into a dimensionless constant by multiplying K_L by 10^6 (Nnaji et al., 2021; Milonjić, 2007). The values of ΔH^0 and entropy change ΔS^0 were calculated from the slope and intercept values of the plot *Ln* K_o versus $1/T_K$ (Fig. S.3). Table 2 presents the thermodynamic parameters.

Table 2 shows negative values of ΔG^0, which means a spontaneous

Table 2
Thermodynamic parameters at various temperatures for As(V) adsorption onto iron-coated cork granulates (S/L = 2.5 g L^{-1}, pH = 3, time = 48 h).

T (K)	$1/T_K$ (10^{-3})	$Ln\ K_o$	ΔG^0 (kJ mol^{-1})	ΔH^0 (kJ mol^{-1})	ΔS^0 (J mol^{-1} K^{-1})
283	3.53	14.4	-34 ± 24	37 ± 24	250 ± 80
293	3.41	15.5	-37 ± 24		
303	3.30	15.4	-39 ± 24		

and feasible process at all three temperatures. In addition, the positive value of ΔH^0 and the decrease of ΔG^0 with increasing temperature confirm that the process is endothermic and becomes more favorable when temperature increases from 10 to 30 °C. The positive value of ΔS^0 suggests that the degree of free active sites increased at the solid/liquid interface during arsenate adsorption onto ICG.

An endothermic process was also the adsorption of arsenate by dried plants (Chiban et al., 2016), coal mine drainage sludge adsorbent (Kim et al., 2021), and metal-impregnated biochar (Rahman et al., 2021). Nevertheless, the adsorption of arsenic on clay minerals (Mohapatra et al., 2007) and on GAC (Mondal et al., 2007) was found to be an exothermic process, where the temperature increase provided a negative effect in As(V) uptake.

3.2. Fixed-bed column adsorption experiments

The capacity of ICG to remove arsenic in continuous mode was investigated at lab-scale fixed-bed column experiments. Several parameters such as bed height, flow rate, temperature, pH and adsorbate initial concentration can influence the adsorption performance and breakthrough curves. Thus, to manage the fixed-bed column in the best way, treatment efficiency was evaluated in different conditions. The results are discussed in the following sections.

3.2.1. Optimization of fixed-bed column

The optimization of the fixed-bed column operational parameters, such as bed height, flow rate, and temperature, was planned by a 2^3 full factorial design with eight experiments corresponding to the runs presented in Table 1. The time parameters are shown in this work either in hours or in minutes to simplify the comparison with other articles and to provide better visualization of the results.

In all runs, the initial As(V) concentration was set as 1 mg L^{-1} at a pH = 3, which was found to be the optimal pH value for arsenate batch adsorption onto ICG, according to previously published results (Pintor et al., 2018). The effluent samples were collected from the column every one or two hours for arsenate concentration measurement.

Each fixed-bed column run performance was assessed in terms of the experimental breakthrough curve parameters. Table 3 presents the values of the BTC experimental parameters for each experiment selected for the 2^3 factorial design.

These eleven variables (except MTZ) was applied as a dependent variable for an ANOVA statistical study. Table 4 presents the ANOVA tables with significant ($p < 0.05$) results, and the others ($p > 0.05$) can be found in Table S.2.

The ANOVA results (Table 4) allow to conclude that (i) the flow rate factor (Q) significantly influences ($p < 0.05$) the breakthrough time (t_b) and the saturation time (t_s), and (ii) the bed height (Z) factor significantly affects ($p < 0.05$) the breakthrough time (t_b), the treated volume at breakthrough (V_b), and the MTZ/Bed height ratio. The main effects plots for each of these parameters are shown in Fig. S.4.

According to Fig. S.4, it is possible to conclude that, as it would be expected, the flow rate (Q) and the breakthrough time (t_b) are inversely proportional in the studied range, as well as the flow rate and the saturation time (t_s). Therefore, increased values of t_b and t_s are expected in a fixed-bed column run with low values of flow rate. Other studies identified the same effect of flow rate on t_b (Ranjan et al., 2009; Sawood and Gupta, 2020) and t_s (Ranjan et al., 2009; Singh et al., 2014) in

Table 4
ANOVA tables with significant ($p < 0.05$) results for the 2^3 factorial design using BTC parameters as response variables: a) breakthrough time (t_b), b) saturation time (t_s); c) treated volume at breakthrough (V_b); and, d) MTZ/Bed height ratio.

Factor	DF	Adj SS	Adj MS	F-Value	P-Value
a)					
Q	**1**	**325.7**	**325.7**	**10.4**	**0.03**
Z	**1**	**419.7**	**419.7**	**13.4**	**0.02**
T	1	96.2	96.2	3.1	0.15
Error	4	124.9	31.2		
Total	7	966.6			
b)					
Q	**1**	**3528.0**	**3528.0**	**11.9**	**0.03**
Z	1	1104.5	1104.5	3.7	0.13
T	1	364.5	364.5	1.2	0.33
Error	4	1186.5	296.6		
Total	7	6183.5			
c)					
Q	1	0.1	0.1	0.0	0.90
Z	**1**	**86.6**	**86.6**	**20.3**	**0.01**
T	1	14.9	14.9	3.5	0.14
Error	4	17.0	4.3		
Total	7	118.6			
d)					
Q	1	0.000	0.000	0.0	0.96
Z	**1**	**0.03**	**0.03**	**20.5**	**0.01**
T	1	0.006	0.006	4.7	0.10
Error	4	0.005	0.001		
Total	7	0.04			

Table 3
Experimental BTC parameters values observed in each column adsorption experiment from 2^3 factorial design.

Run #	t_b (h)	t_s (h)	q_b (mg g^{-1})	q_s (mg g^{-1})	BV_b	BV_s	V_b (L)	V_s (L)	y_b (%)	y_s (%)	*MTZ (cm)*	*MTZ/Bed height*
1	20.6 ± 0.8	85	1.7 ± 0.2	3.5 ± 0.7	229 ± 9	945 ± 87	6.7 ± 0.3	27.8 ± 0.1	99.95 ± 0.03	51 ± 6	4.5 ± 0.4	0.76 ± 0.09
2	5.0 ± 0.4	25	0.84 ± 0.08	2.4 ± 0.2	108 ± 14	535 ± 49	3.2 ± 0.3	15.75 ± 0.08	99.75 ± 0.08	57 ± 3	4.8 ± 0.6	0.8 ± 0.1
3	26.3 ± 0.8	78	1.07 ± 0.08	2.1 ± 0.3	146 ± 10	433 ± 25	8.6 ± 0.3	25.5 ± 0.1	99.80 ± 0.05	65 ± 4	8.0 ± 0.4	0.66 ± 0.04
4	20.2 ± 0.4	47	1.7 ± 0.1	2.8 ± 0.3	216 ± 14	503 ± 29	12.8 ± 0.3	29.6 ± 0.1	99.79 ± 0.04	68 ± 3	6.8 ± 0.3	0.57 ± 0.04
5	12.1 ± 0.4	44	2.2 ± 0.1	4.3 ± 0.7	254 ± 25	927 ± 86	7.5 ± 0.3	27.3 ± 0.1	99.99 ± 0.01	54 ± 5	4.4 ± 0.4	0.73 ± 0.09
6	45.3 ± 0.8	122	1.8 ± 0.2	3.4 ± 0.5	252 ± 16	678 ± 39	14.8 ± 0.9	39.9 ± 0.1	99.82 ± 0.03	69 ± 4	7.5 ± 0.3	0.63 ± 0.04
7	18 ± 1	70	1.6 ± 0.2	3.7 ± 0.6	197 ± 23	778 ± 72	5.8 ± 0.4	22.9 ± 0.1	99.67 ± 0.05	57 ± 7	4.5 ± 0.5	0.7 ± 0.1
8	21.5 ± 0.8	71	1.9 ± 0.1	4.4 ± 0.4	226 ± 16	748 ± 43	13.3 ± 0.6	44.1 ± 0.1	99.45 ± 0.08	68 ± 3	8.4 ± 0.5	0.70 ± 0.05

(± standard error of the mean)

fixed-bed columns for arsenic removal. The effect of flow rate in adsorption is related to the residence time, as lower values of flow rate increase the time available for the adsorbate to access the adsorption sites in the adsorbent surface.

As presented in Fig. S.4, bed height (Z) and breakthrough time (t_b) are directly proportional in the studied range, as well as bed height and treated volume at breakthrough (V_b). Therefore, increased values of t_b and V_b are expected in a fixed-bed column with a high bed height. The bed height influences the exhaustion time because it provides more binding sites for the adsorbate to contact with the adsorbent (Ranjan et al., 2009).

The fixed-bed column efficiency is also expressed in terms of MTZ, which should be minimized for best adsorption performance (Mantovaneli et al., 2004), for instance, through flow rate decrease and bed height increase (Díaz-Blancas et al., 2020). The unutilized bed height can be expressed in terms of MTZ/bed height ratio when comparing different bed height values. The assays with the longest bed height of 12 cm achieved the lowest values of the ratio, $0.57 \leq$ MTZ/Bed height ≤ 0.70. For a bed height of 6 cm we found $0.73 \leq$ MTZ/Bed height ≤ 0.80. This is in accordance with DOE results (Fig. S.4. d), which show that bed height statistically influences ($p < 0.05$) MTZ/Bed height in an inversely proportional way.

So, from the DOE results of the lab-scale fixed-bed column setup, the optimized flow rate and bed height factors are 5 mL min^{-1} and 12 cm (6 g mass), respectively. As expected, they correspond to the highest empty bed contact time (EBCT) value of 11.8 min. Research on the adsorption kinetics of As(V) at 1 mg L^{-1} onto ICG showed a high adsorption rate in the first 15 min (Pintor et al., 2020b), which confirms that an EBCT of approximately 15 min is required to promote a high rate of arsenic adsorption in continuous mode.

Moreover, DOE results presents that there is not a significant influence ($p < 0.05$) on the column performance as regards the following parameters: adsorption capacity at breakthrough (q_b), adsorption capacity at the saturation point (q_s), bed volume treated at breakthrough (BV_b), bed volume treated at the saturation point (BV_s), saturation volume (V_s), arsenic removal at breakthrough (y_b), and arsenic removal at saturation (y_s). This means that although the previously defined parameters are preferable, the column can also be operated at less-optimal parameters with effectiveness.

Regardless of the temperature effect observed in batch mode adsorption onto ICG (Fig. 2), this factor did not present a statistically significant influence ($p < 0.05$) on any experimental BTC parameters reported in Table 3.

Nevertheless, temperature affected the iron amount leached from the adsorbent, as shown in Fig. S.5 (10 and 20 °C) and Fig S.6 (30 °C). In column assays conducted at pH 3, flow rate of 5 mL min^{-1}, and As(V) initial concentration of 1 mg L^{-1}, the average total iron concentration in the effluent was 0.3 ± 0.1 and 0.5 ± 0.1 mg L^{-1} for experiments at 10 and 20 °C, respectively. Throughout those assays, a smooth decay behavior is observed in the iron concentration, reaching a minimum value at saturation time.

For experiments conducted at 30 °C, an increase in iron leaching was observed approximately until breakthrough time, when it reaches maximum value, followed by a decay until saturation time (Fig. S.6). For the assays with a breakthrough time of 12 h and 45 h, the maximum total iron concentration in the effluent was achieved after 14 h and 42 h operation, respectively. From breakthrough to saturation, there may be a blockage of the iron dissolution due to occupation of the adsorption sites by the arsenic oxyanions or even by small iron-arsenic micro-precipitates. These could justify the decrease and, ultimately, absence of Fe in the effluent by saturation time. The adsorption mechanism is better observed in the experiments conducted at 30 °C, which is the most favorable adsorption temperature in the range of 10 – 30 °C according to the endothermic behavior of ICG arsenic adsorption (Section 3.1.2).

3.2.2. Analysis of breakthrough curves (BTC)

The Thomas (Eq. (13)), Yoon-Nelson (Eq. 14)), and Yan (Eq. (15)) models were fitted to experimental data from 2^3 factorial design fixed-bed column assays (Section 3.2.1) by nonlinear regression. The results are displayed in Table 5, and BTC's are presented in Fig. S.7.

Due to the fact that the Thomas and Yoon-Nelson models are mathematically equivalent (Chu, 2020), their correlation parameters and standard error are equal, as well as the theoretical breakthrough curves. The Yan model better represents the experimental data, considering the higher values of correlation coefficient ($R^2 \geq 0.97$) and lower values of standard error ($SE \leq 0.07$). According to Table 5, theoretical adsorption capacity values from Yan (Q_{YA}) model were slightly smaller than the experimental ones (q_{exp}). Maximum adsorption capacities predicted by the Thomas model were closer to q_{exp}. The divergence in predicted and experimental adsorption parameters can be related to deviations of the model fittings from experimental data at the beginning and at the end of the experimental curve, where saturation is hardly achieved (Jaria et al., 2019).

3.2.3. Effect of temperature

Batch studies revealed that the As(V) adsorption was influenced by temperature in the range 10–30 °C (Section 3.1). Nevertheless, DOE results (Section 3.2.1) showed no evidence of a significant temperature effect ($p > 0.05$) in the column performance, for the same temperature range. To obtain an optimal temperature value, an intermediate value of temperature (20 °C) was tested in the optimal conditions of 5 mL min^{-1} flow rate and 12 cm bed height. The breakthrough curves for 20 and 30 °C were very similar, with breakthrough times of 45.6 ± 0.7 h and 45.3 ± 0.8 h, respectively. Fig. 3 presents the temperature effect in breakthrough curves from the column assays carried out at temperatures 10, 20 and 30 °C. As expected, the assay conducted at 10 °C led to the poorest performance, with a breakthrough time of 26.3 ± 0.8 h.

Since the fixed-bed column performances at 20 and 30 °C were close, the temperature of 20 °C was chosen to be applied in the following assays because it is usually closer to environmental conditions.

3.2.4. Effect of pH

Previous studies in batch mode showed that As(V) and As(III) adsorption onto ICG is highly dependent on pH (Pintor et al., 2018). For As(III), a maximum uptake was obtained at pH 9. Oppositely, for As(V), the increase of pH from 3.0 to 7.0 caused a proportional decrease in adsorption capacity of 50%, from approximately 4.0 mg g^{-1} to 2.0 mg g^{-1} (Pintor et al., 2018). In the same study a pH_{PZC} of ICG close to 6 was determined.

The inverse trends on arsenate and arsenite uptake observed in batch mode were also observed in continuous mode (Fig. 4). The experimental and theoretical breakthrough parameters for As(V) and As(III) are found in Table S.3.

The pH increase caused an inversely proportional effect ($R^2 > 0.9$ on linear regressions) on all BTC parameters for As(V) uptake (Fig. S.8), except for arsenic removal at breakthrough (yb), which remained above 99.8%. Adsorption capacity predicted by the Yan model was reduced from 3.8 ± 0.3–0.56 ± 0.04 mg g^{-1} with pH increment from 3 to 9. The same increment in pH reduced breakthrough time from 45.6 ± 0.7 h to 7.1 ± 0.5 h (Table S.3).

The reduction in As(V) adsorption caused by increasing the pH was also reported in other column operation studies using different adsorbents (Nguyen et al., 2020) and justified by the competition of OH^- ion with arsenate ions (Tiwari and Chaudhari, 2020). At pH values lower than the pH_{PZC} of ICG, the positively charged surface of ICG can more efficiently interact with $H_2AsO_4^-$ ions, the contrary of what occurs at high pH, in which the negatively charged ICG surface repulses the more electronegative $HAsO_4^{2-}$ (Pintor et al., 2018).

In contrast, the increase in pH from 7 to 9 resulted in the rise of As (III) adsorption onto ICG. It was previously observed in the batch results (Pintor et al., 2018) that at this pH range, the As(III) is mostly present as

Table 5
Parameters of Thomas, Yoon-Nelson and Yan models.

Run	1	2	3	4	5	6	7	8
Thomas model								
K_{TH} (10^{-3})	2.0 ± 0.2	6.7 ± 0.7	2.5 ± 0.2	4.4 ± 0.4	5.5 ± 0.7	1.8 ± 0.2	2.5 ± 0.2	2.1 ± 0.2
q_{TH} (mg g^{-1})	3.3 ± 0.5	2.3 ± 0.5	2.0 ± 0.2	2.7 ± 0.3	3.9 ± 0.6	3.3 ± 0.4	3.6 ± 0.4	4.3 ± 0.4
q_{exp} (mg g^{-1})	3.5 ± 0.7	2.4 ± 0.2	2.1 ± 0.3	2.8 ± 0.3	4.3 ± 0.7	3.4 ± 0.5	3.7 ± 0.6	4.4 ± 0.4
R^2	0.942	0.961	0.988	0.979	0.968	0.970	0.976	0.971
SE	0.09	0.07	0.04	0.05	0.07	0.06	0.06	0.06
Yoon-Nelson model								
K_{YN} (10^{-3})	1.5 ± 0.1	5.3 ± 0.5	1.8 ± 0.1	3.6 ± 0.2	4.7 ± 0.4	1.33 ± 0.07	2.1 ± 0.1	1.9 ± 0.1
t_{YN} 50% (min)	2458 ± 302	815 ± 109	3013 ± 182	1882 ± 177	1320 ± 174	4917 ± 350	2317 ± 192	2852 ± 231
t_{exp} 50% (min)	2255 ± 58	797 ± 11	3001 ± 89	1798 ± 18	1287 ± 17	4730 ± 81	2133 ± 32	2694 ± 60
R^2	0.942	0.961	0.988	0.979	0.968	0.970	0.976	0.971
SE (m g^{-1})	0.09	0.07	0.04	0.05	0.07	0.06	0.06	0.06
Yan model								
a_{ya}	3.4 ± 0.2	4.3 ± 0.3	5.4 ± 0.2	6.5 ± 0.3	5.5 ± 0.4	6.2 ± 0.2	4.6 ± 0.2	5.1 ± 0.3
Q_{ya} (mg g^{-1})	3.1 ± 0.3	2.2 ± 0.1	2.0 ± 0.2	2.7 ± 0.2	3.9 ± 0.3	3.2 ± 0.3	3.5 ± 0.3	4.2 ± 0.3
q_{exp} (mg g^{-1})	3.5 ± 0.7	2.4 ± 0.2	2.1 ± 0.3	2.8 ± 0.3	4.3 ± 0.7	3.4 ± 0.5	3.7 ± 0.6	4.4 ± 0.4
SE (mg g^{-1})	0.07	0.05	0.02	0.04	0.05	0.05	0.04	0.05
R^2	0.967	0.980	0.994	0.990	0.980	0.983	0.991	0.981

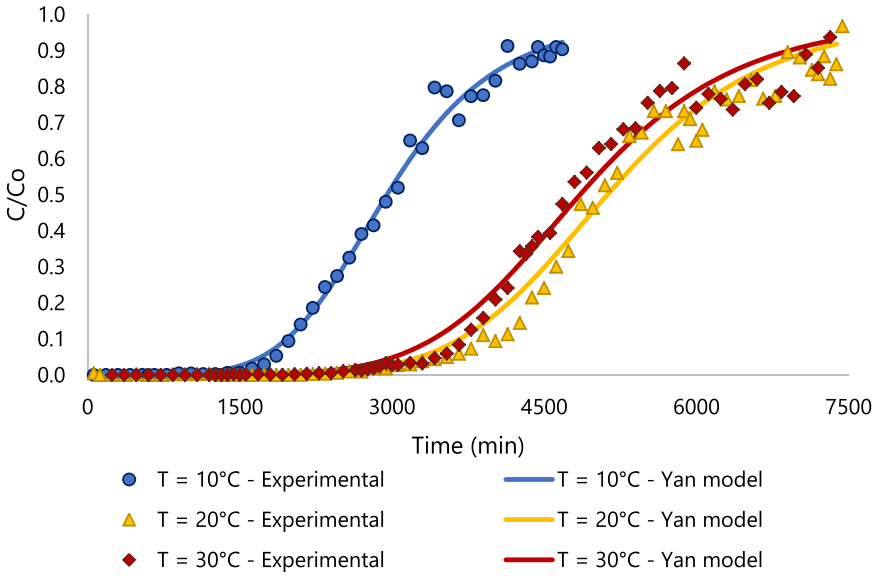

Fig. 3. Theoretical (Yan model) and experimental breakthrough curves of arsenic adsorption onto ICG at different temperatures: 10, 20 and 30 °C (bed height: 12 cm, flow rate: 5 mL min^{-1}, pH 3.0, $C_{oAs(V)}$ 1 mg L^{-1}).

neutral arsenious acid (H_3AsO_3), and its adsorption is favorable when the surface of adsorbent is close to neutral, from 6 to 9, which is close to pH_{PZC} (Pintor et al., 2018; Maji et al., 2012). In addition, it was argued that the beginning of H_3AsO_3 dissociation to $H_2AsO_3^-$ at $pK_a = 9.2$ could induce to an increase in electrostatic repulsion among As(III) and negatively charged adsorbent surface at high values of pH.

Some studies also reported the pH effect on As(III) adsorption, showing analogous trends for arsenite adsorption onto ICG (Maji et al., 2012; Navarathna et al., 2019) and others indicate different behavior where As(V) and As(III) are identically influenced by pH (Ali, 2018).

The pH has an important effect on the iron leaching from ICG. The concentration of iron leached in the assays carried at pH values of 7 and 9, at 20 °C, reached a maximum value of 0.08 mg L^{-1}. In contrast, Fe concentrations of 0.32–0.96 mg L^{-1} were observed in the effluent from the assay at pH 3. However, these values are still much lower than the Fe leached in the batch assay conducted at identical pH and temperature of 20 °C (Section 3.1.3). The fact that a very low concentration of iron was released from ICG reduces the concern raised in Section 3.1.1 of iron being a hindrance in the application of ICG, considering the adsorbent is more likely to be used at pH conditions of 6–9.

Table 6 summarizes literature results from fixed-bed columns operating at an inlet concentration of 1 mg L^{-1}, including the ones obtained in the current study with ICG. The ICG adsorption capacity achieved an excellent value comparing to other modified adsorbents, such as Zr-type adsorbent, iron-mixed mesoporous pellet, and thioglycolated sugarcane carbon. However, in terms of breakthrough time, the values observed for ICG, at similar pH value, were inferior to other iron-based adsorbents, such as magnetic binary oxide particles and iron modified bauxite. It is important to note, however, that the breakthrough time depends highly on the column configuration.

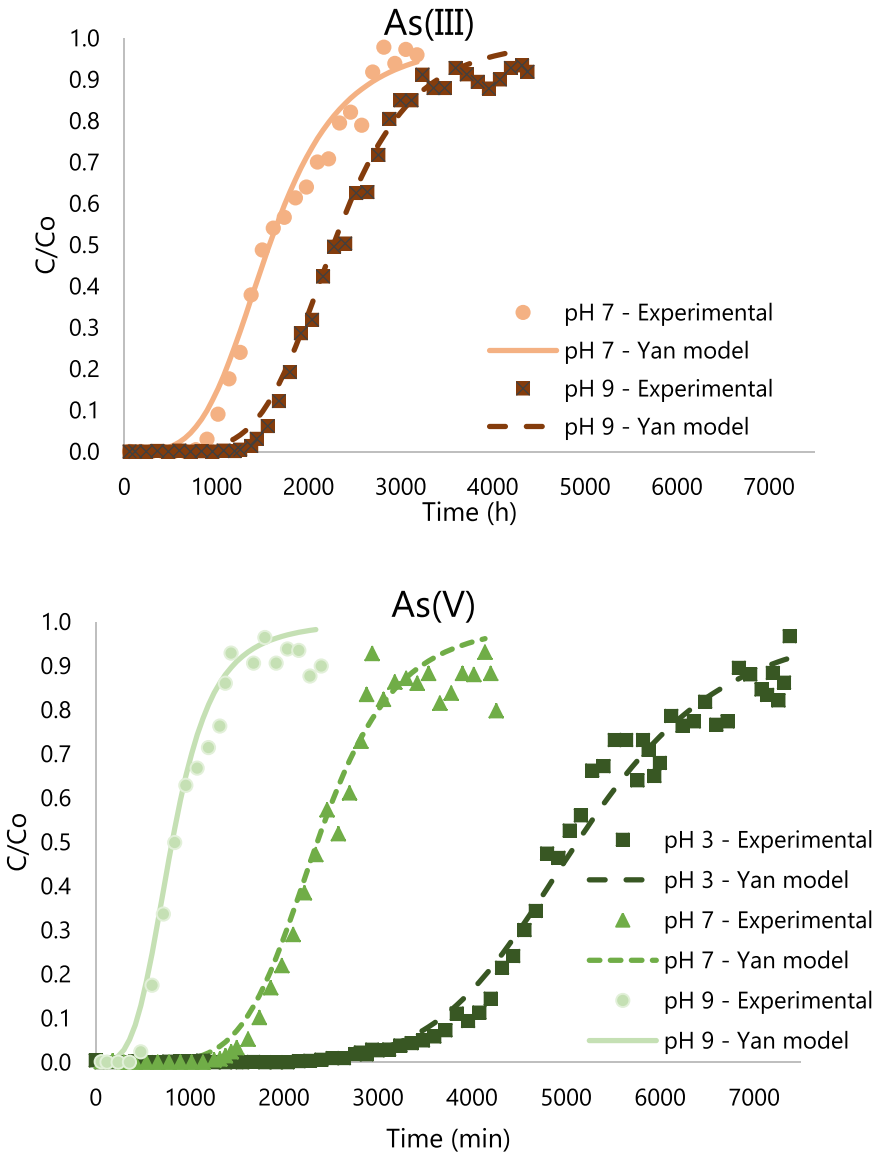

Fig. 4. Experimental and theoretical (Yan model) breakthrough curves of arsenic adsorption onto ICG for different pH values: a) As(III), pH of 7 and 9; b) As(V) pH of 3, 7 and 9.

3.2.5. Effect of initial concentration

To assess the effect of inlet arsenic concentration in fixed-bed adsorption, new assays were carried out with As(V) and As(III), separately, with initial concentrations of 0.1 and 1 mg L^{-1}, at 20 ± 0.5 °C and pH 7.0 ± 0.1. The column tests were conducted at the optimal laboratory-scale column conditions. The results are presented in Table S.4 and Fig. 5.

The reduction in inlet concentration of 1.0–0.1 mg L^{-1} caused an inversely proportional effect in t_b, t_s, BV_b, BV_s, V_b and V_s, for arsenate adsorption. The adsorption capacity at breakthrough, q_b, reduced from 1.1 mg g^{-1} to 0.8 mg g^{-1} for As(V) and remained unchanged for As(III), as 0.5 mg g^{-1}. The maximum adsorption capacity predicted by the Yan model, Q_{ya}, decreased from 1.9 ± 0.1–1.5 ± 0.2 mg g^{-1} and from 1.1 ± 0.1–0.8 ± 0.1 mg g^{-1}, for As(V) and As(III), respectively. Even though Q_{ya} values for As(V) are approximately two times higher than Q_{ya} values for As(III), it is still feasible to remove arsenite by ICG adsorption in continuous mode without oxidizing it to arsenate. The column assay operated at 0.1 mg L^{-1} achieved the lowest value of MTZ, of 5.9, with a MTZ/Bed height ratio of 0.49, which confirms the overall good efficiency of the ICG adsorption column for arsenite removal.

From the synthetic arsenic inlet solution used in this work, the ones with the lowest concentration of 0.1 mg L^{-1} at neutral pH value were the closest to real arsenic-contaminated groundwaters used for human consumption, which are usually found at pH 6.5–8 and in the range of 0.1–0.3 mg L^{-1}.

For the As(III) influent at 0.1 mg L^{-1}, effluent concentrations under 10 μg L^{-1} and 50 μg L^{-1} were observed for 569 and 861 bed volumes, respectively. In comparison to other fixed-bed column performances under similar conditions, we achieved better results than Fe-modified GAP (granular attapulgite-supported), which treated 175 and 249 BVs under 10 μg L^{-1} and 50 μg L^{-1}, respectively (Yin et al., 2017); but not as good as zirconium metal organic frameworks (UiO-66) that treated 1775 BVs before the effluent reached 10 μg L^{-1}.

For the influent with 0.1 mg L^{-1} As(V), the ICG fixed-bed column provided an effluent under 10 μg L^{-1} and 50 μg L^{-1} for 895 and 1633 bed volumes, respectively. The values were higher than those achieved by iron oxide-coated fungal biomass (IOCB)) which treated 800 BV before attaining 10 μg L^{-1} at pH 6 (Pokhrel and Viraraghavan, 2008); higher also than natural laterite from Thach That (NLTT) when treating approximately 500 BV before breakthrough at 10 μg L^{-1}, at pH 7 (Nguyen et al., 2021); but inferior to the results obtained with GAC-Fe, which reached 10 μg L^{-1} after 1494 BV of treated effluent (Kalaruban et al., 2019).

Table 6
Fixed-bed column performances reported in other works for As(III) and As(V) removal with an initial concentration of 1 mg L^{-1}.

Adsorbent	Arsenic species	pH	Maximum adsorption capacity (mg g^{-1})	Breakthrough time at 0.01 mg L^{-1} (h)	Ref.
Magnetic binary oxide particles (MBOP) using chitosan	As(III)	7.23	4.67	26	(Dhoble et al., 2017)
Iron modified calcined bauxite (MCB)	As(III)	6.8 ± 0.4	0.490	50	(Bhakat et al., 2007)
Zr-type adsorbent from nonwoven cotton fabric	As(V)	2	0.749	–	(Hoshina et al., 2012)
Iron-mixed mesoporous pellet	As(III) As(V)	7 ± 0.1	0.454 0.340	11 6	(Te et al., 2018)
Thioglycolated sugarcane carbon (TSCC)	As(III) As(V)	6	0.073 0.072	~90	(Roy et al., 2013)
Agglomerated nanoparticles of Mn-incorporated Fe(III) oxide (MNFO)	As(III)	7.5	3.34	–	(Ghosh et al., 2014)
Iron-coated cork granulates (ICG)	As (III) As(III) As(V) As(V)	7 9 3 7	1.2 ± 0.2 1.8 ± 0.4 3.9 ± 0.5 2.0 ± 0.3	13.7 ± 0.4 22.7 ± 0.7 45.6 ± 0.7 22.5 ± 0.6	This study

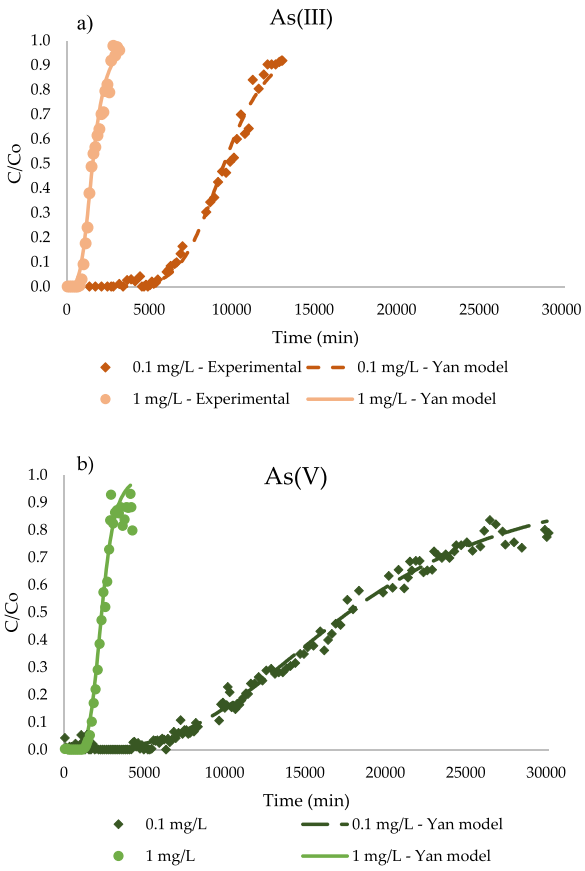

Fig. 5. Experimental and theoretical (Yan model) breakthrough curves of arsenic adsorption onto ICG with initial concentration values of 0.1 and 1 mg L^{-1} (pH 7 and $T = 20$ °C): a) As(III); b) As(V).

4. Conclusion

Iron-coated cork granulates (ICG) were proven to efficiently remove arsenic from aqueous solution at various conditions, including the environmentally relevant conditions of pH 7 and arsenic inlet concentration of 0.1 mg L^{-1}. In these conditions, the effluent exceeded 10 μg L^{-1} and 50 μg L^{-1} only after 895 and 1633 bed volumes, respectively, for As(V), and 569 and 861 bed volumes, respectively, for As(III).

Breakthrough curves were best described by the Yan model with most of the determination coefficients above 0.98, although Thomas and Yoon-Nelson models showed good nonlinear fits. Maximum adsorption capacities in continuous mode predicted by Yan model were 4.2 ± 0.3 mg As(V) g^{-1} ICG and 1.6 ± 0.2 mg As(III) g^{-1} ICG for C_o of 1 mg L^{-1}, higher than those obtained in batch experiments for low equilibrium concentration.

Bed height and flow rate provided a statistically significant influence on some BTC experimental parameters; however, no statistically significant effect of temperature was observed in the 10–30 °C range. On the contrary, in batch studies, a directly proportional effect of temperature on isotherm parameters predicted by Langmuir and Freundlich models was observed. A maximum adsorption capacity of 6.9 ± 0.1 mg As(V) g^{-1} ICG at 30 °C was calculated using the Langmuir fit. Thermodynamic studies confirmed the adsorption process to be endothermic, spontaneous, and feasible.

In accordance with earlier batch studies, pH variation caused a proportional change in BTC parameters, with 3 and 9 being more favorable pH values for As(V) and As(III), respectively. However, good efficiency was still observed at pH 7 for both species, which is the value recommended for waters with arsenate and arsenite co-contamination. At pH 7, low iron leaching from the adsorbent was also observed. The variation in initial arsenic concentration also influenced the majority of BTC parameters, as expected.

Further work should investigate the removal of arsenic using the ICG fixed-bed column in real waters, such as contaminated groundwater and mining runoff. Forthcoming studies should also explore possibilities for regeneration of the exhausted bed and its sustainable disposal.

Funding

This work was financially supported by LA/P/0045/2020 (ALiCE), UIDB/50020/2020 and UIDP/50020/2020 (LSRE-LCM), funded by national funds through FCT/MCTES (PIDDAC). A. Pintor acknowledges her Junior Researcher contract [CEECIND/01485/2017] by FCT. M. Carneiro acknowledges her Ph.D. scholarship by FCT [2020.07233. BD].

CRediT authorship contribution statement

Mariko A. Carneiro: Methodology, Validation, Formal analysis, Investigation, Writing – original draft, Visualization. **Ariana M.A. Pintor**: Conceptualization, Methodology, Writing – review & editing, Supervision. **Rui A.R. Boaventura**: Writing – review & editing, Funding acquisition. **Cidália M.S. Botelho**: Resources, Writing – review & editing, Funding acquisition.

Declaration of Competing Interest

The authors declare that they have no known competing financial interests or personal relationships that could have appeared to influence the work reported in this paper.

Appendix A. Supporting information

Supplementary data associated with this article can be found in the online version at doi:10.1016/j.jhazmat.2022.128657.

References

Ali, I., 2018. Microwave assisted economic synthesis of multi walled carbon nanotubes for arsenic species removal in water: batch and column operations. J. Mol. Liq. 271, 677–685. https://doi.org/10.1016/j.molliq.2018.09.021.

Asere, T.G., Stevens, C.V., Du Laing, G., 2019. Use of (modified) natural adsorbents for arsenic remediation: a review. Sci. Total Environ. 676, 706–720.

Bacelo, H., et al., 2020. Performance and prospects of different adsorbents for phosphorus uptake and recovery from water. Chem. Eng. J. 381, 122566 https://doi.org/10.1016/j.cej.2019.122566.

Bhakat, P.B., Gupta, A.K., Ayoob, S., 2007. Feasibility analysis of As(III) removal in a continuous flow fixed bed system by modified calcined bauxite (MCB). J. Hazard. Mater. 139 (2), 286–292. https://doi.org/10.1016/j.jhazmat.2006.06.037.

Brion-Roby, R., et al., 2018. Investigation of fixed bed adsorption column operation parameters using a chitosan material for treatment of arsenate contaminated water. J. Environ. Chem. Eng. 6 (1), 505–511. https://doi.org/10.1016/j.jece.2017.12.032.

Brion-Roby, R., et al., 2018. Development and treatment procedure of arsenic-contaminated water using a new and green chitosan sorbent: kinetic, isotherm, thermodynamic and dynamic studies. Pure Appl. Chem. 90 (1), 63–77. https://doi.org/10.1515/pac-2017-0305.

Carneiro, M.A., et al., 2021. Current trends of arsenic adsorption in continuous mode: literature review and future perspectives. Sustainability 13 (3), 1186.

Chatterjee, A., Schiewer, S., 2011. Biosorption of cadmium(II) ions by citrus peels in a packed bed column: effect of process parameters and comparison of different breakthrough curve models. CLEAN Soil Air Water 39 (9), 874–881. https://doi.org/10.1002/clen.201000482.

Chen, C.-C., Chung, Y.-C., 2006. Arsenic removal using a biopolymer chitosan sorbent. J. Environ. Sci. Health Part A 41 (4), 645–658. https://doi.org/10.1080/10934520600575044.

Chiban, M., et al., 2016. Equilibrium and thermodynamic studies for the removal of As (V) ions from aqueous solution using dried plants as adsorbents. Arab. J. Chem. 9, S988–S999. https://doi.org/10.1016/j.arabjc.2011.10.002.

Chu, K.H., 2020. Breakthrough curve analysis by simplistic models of fixed bed adsorption: in defense of the century-old Bohart-Adams model. Chem. Eng. J. 380, 122513 https://doi.org/10.1016/j.cej.2019.122513.

European Commission, 2008. Council Directive 98/83/EC of 3 November 1998 on the quality of water intended for human consumption 2008, Off. J. Eur. Commun. L. p. 32.

Dhoble, R.M., et al., 2017. Removal of arsenic(III) from water by magnetic binary oxide particles (MBOP): experimental studies on fixed bed column. J. Hazard. Mater. 322, 469–478. https://doi.org/10.1016/j.jhazmat.2016.09.075.

Dias, A.C., Fontes, M.P.F., 2020. Arsenic (V) removal from water using hydrotalcites as adsorbents: a critical review. Appl. Clay Sci. 191, 105615.

Díaz-Blancas, V., et al., 2020. Evaluation of mass transfer mechanisms involved during the adsorption of metronidazole on granular activated carbon in fixed bed column. J. Water Process Eng. 36, 101303 https://doi.org/10.1016/j.jwpe.2020.101303.

Freundlich, H., 1907. Über die Adsorption in Lösungen. Z. Phys. Chem. 57U (1), 385–470. https://doi.org/10.1515/zpch-1907-5723.

Ghosh, A., Chakrabarti, S., Ghosh, U.C., 2014. Fixed-bed column performance of Mn-incorporated iron(III) oxide nanoparticle agglomerates on As(III) removal from the spiked groundwater in lab bench scale. Chem. Eng. J. 248, 18–26. https://doi.org/10.1016/j.cej.2014.03.010.

Hao, L., et al., 2018. A critical review on arsenic removal from water using iron-based adsorbents. RSC Adv. 8 (69), 39545–39560.

Hoshina, H., et al., 2012. Adsorbent for Arsenic (V) removal synthesized by radiation-induced graft polymerization onto nonwoven cotton fabric. Int. J. Org. Chem. 2, 173–177.

Jaria, G., et al., 2019. Fixed-bed performance of a waste-derived granular activated carbon for the removal of micropollutants from municipal wastewater. Sci. Total Environ. 683, 699–708. https://doi.org/10.1016/j.scitotenv.2019.05.198.

Kalaruban, M., et al., 2019. Iron-impregnated granular activated carbon for arsenic removal: application to practical column filters. J. Environ. Manag. 239, 235–243. https://doi.org/10.1016/j.jenvman.2019.03.053.

Kim, D., et al., 2021. Arsenic adsorption on two types of powdered and beaded coal mine drainage sludge adsorbent. Chemosphere 272, 129560. https://doi.org/10.1016/j.chemosphere.2021.129560.

Langmuir, I., 1918. The adsorption of gases on plane surfaces of glass, mica and platinum. J. Am. Chem. Soc. 40 (9), 1361–1403. https://doi.org/10.1021/ja02242a004.

Lata, S., Samadder, S., 2016. Removal of arsenic from water using nano adsorbents and challenges: a review. J. Environ. Manag. 166, 387–406.

Lim, K.T., Shukor, M.Y., Wasoh, H., 2014. Physical, chemical, and biological methods for the removal of arsenic compounds, 503784-503784 BioMed Res. Int. 2014. https://doi.org/10.1155/2014/503784.

Lin, S., et al., 2018. A novel biodegradable arsenic adsorbent by immobilization of iron oxyhydroxide (FeOOH) on the root powder of long-root Eichhornia crassipes. Chemosphere 192, 258–266. https://doi.org/10.1016/j.chemosphere.2017.10.163.

Liu, Z., Zhang, F.-S., Sasai, R., 2010. Arsenate removal from water using Fe3O4-loaded activated carbon prepared from waste biomass. Chem. Eng. J. 160 (1), 57–62. https://doi.org/10.1016/j.cej.2010.03.003.

Maiti, A., et al., 2010. Removal of As(V) using iron oxide impregnated carbon prepared from Tamarind hull. J. Environ. Sci. Health Part A 45 (10), 1207–1216. https://doi.org/10.1080/10934529.2010.493783.

Maji, S.K., et al., 2012. Fixed bed adsorption of As(III) on iron-oxide-coated natural rock (IOCNR) and application to real arsenic-bearing groundwater. Chem. Eng. J. 203, 285–293. https://doi.org/10.1016/j.cej.2012.07.033.

Mantovaneli, I., et al., 2004. The effect of temperature and flow rate on the clarification of the aqueous Stevia-extract in a fixed-bed column with zeolites. Braz. J. Chem. Eng. 21 (3), 449–458.

Milonjić, S.K., 2007. A consideration of the correct calculation of thermodynamic parameters of adsorption. J. Serb. Chem. Soc. 72 (12), 1363–1367.

Mohapatra, D., et al., 2007. Arsenic adsorption mechanism on clay minerals and its dependence on temperature. Korean J. Chem. Eng. 24 (3), 426–430. https://doi.org/10.1007/s11814-007-0073-z.

Mondal, M.K., Garg, R., 2017. A comprehensive review on removal of arsenic using activated carbon prepared from easily available waste materials. Environ. Sci. Pollut. Res. 24 (15), 13295–13306.

Mondal, P., Balomajumder, C., Mohanty, B., 2007. A laboratory study for the treatment of arsenic, iron, and manganese bearing ground water using Fe3+ impregnated activated carbon: effects of shaking time, pH and temperature. J. Hazard. Mater. 144 (1), 420–426. https://doi.org/10.1016/j.jhazmat.2006.10.078.

Natasha, et al., 2021. Health risks of arsenic buildup in soil and food crops after wastewater irrigation. Sci. Total Environ. 772, 145266 https://doi.org/10.1016/j.scitotenv.2021.145266.

Navarathna, C.M., et al., 2019. Removal of Arsenic(III) from water using magnetite precipitated onto Douglas fir biochar. J. Environ. Manag. 250, 109429 https://doi.org/10.1016/j.jenvman.2019.109429.

Nguyen, P.T.T., et al., 2020. Removal of Arsenic from groundwater using lamdong laterite as a natural adsorbent. Pol. J. Environ. Stud. 29 (2), 1305–1314. https://doi.org/10.15244/pjoes/103028.

Nguyen, T.H., et al., 2021. Low-cost laterite-laden household filters for removing arsenic from groundwater in Vietnam and waste management. Process Saf. Environ. Prot. 152, 154–163. https://doi.org/10.1016/j.psep.2021.06.002.

Nnaji, C.C., et al., 2021. Equilibrium and thermodynamic investigation of biosorption of nickel from water by activated carbon made from palm kernel chaff. Sci. Rep. 11 (1), 7808. https://doi.org/10.1038/s41598-021-86932-6.

Patel, H., 2019. Fixed-bed column adsorption study: a comprehensive review. Appl. Water Sci. 9 (3), 1–17.

Pintor, A.M.A., et al., 2012. Use of cork powder and granules for the adsorption of pollutants: a review. Water Res. 46 (10), 3152–3166. https://doi.org/10.1016/j.watres.2012.03.048.

Pintor, A.M.A., et al., 2018. Arsenate and arsenite adsorption onto iron-coated cork granulates. Sci. Total Environ. 642, 1075–1089. https://doi.org/10.1016/j.scitotenv.2018.06.170.

Pintor, A.M.A., et al., 2020a. Removal of antimony from water by iron-coated cork granulates. Sep. Purif. Technol. 233, 116020 https://doi.org/10.1016/j.seppur.2019.116020.

Pintor, A.M.A., et al., 2020b. Complexation mechanisms in arsenic and phosphorus adsorption onto iron-coated cork granulates. J. Environ. Chem. Eng. 8 (5), 104184 https://doi.org/10.1016/j.jece.2020.104184.

Pintor, A.M.A., et al., 2021. Multicomponent adsorption of pentavalent As, Sb and P onto iron-coated cork granulates. J. Hazard. Mater. 406, 124339 https://doi.org/10.1016/j.jhazmat.2020.124339.

Pokhrel, D., Viraraghavan, T., 2008. Arsenic removal in an iron oxide-coated fungal biomass column: analysis of breakthrough curves. Bioresour. Technol. 99 (6), 2067–2071. https://doi.org/10.1016/j.biortech.2007.04.023.

Rahman, M.A., et al., 2021. Removal of arsenate from contaminated waters by novel zirconium and zirconium-iron modified biochar. J. Hazard. Mater. 409, 124488 https://doi.org/10.1016/j.jhazmat.2020.124488.

Ranjan, D., Talat, M., Hasan, S.H., 2009. Rice polish: an alternative to conventional adsorbents for treating arsenic bearing water by up-flow column method. Ind. Eng. Chem. Res. 48 (23), 10180–10185. https://doi.org/10.1021/ie900877p.

Roy, P., et al., 2013. Removal of arsenic(III) and arsenic(V) on chemically modified low-cost adsorbent: batch and column operations. Appl. Water Sci. 3 (1), 293–309. https://doi.org/10.1007/s13201-013-0082-5.

Saha, S., Sarkar, P., 2016. Arsenic mitigation by chitosan-based porous magnesia-impregnated alumina: performance evaluation in continuous packed bed column. Int. J. Environ. Sci. Technol. 13 (1), 243–256. https://doi.org/10.1007/s13762-015-0806-1.

Sarkar, P., et al., 2010. Removal of arsenic from drinking water by ferric hydroxide microcapsule-loaded alginate beads in packed adsorption column. J. Environ. Sci. Health Part A 45 (13), 1750–1757. https://doi.org/10.1080/10934529.2010.513267.

Sawood, G.M., Gupta, S.K., 2020. Arsenate adsorption from aqueous solution using iron-loaded Azadirachta indica roots: batch and fixed-bed column study. Desalin. Water Treat. 203, 292–308. https://doi.org/10.5004/dwt.2020.26233.

Shaji, E., et al., 2021. Arsenic contamination of groundwater: a global synopsis with focus on the Indian Peninsula. Geosci. Front. 12 (3), 101079 https://doi.org/10.1016/j.gsf.2020.08.015.

Sharma, A.K., et al., 2014. Review of arsenic contamination, exposure through water and food and low cost mitigation options for rural areas. Appl. Geochem. 41, 11–33. https://doi.org/10.1016/j.apgeochem.2013.11.012.

Shipley, H.J., et al., 2009. Adsorption of arsenic to magnetite nanoparticles: effect of particle concentration, pH, ionic strength, and temperature. Environ. Toxicol. Chem. 28 (3), 509–515. https://doi.org/10.1897/08-155.1.

Silva, S.P., et al., 2005. Cork: properties, capabilities and applications. Int. Mater. Rev. 50 (6), 345–365. https://doi.org/10.1179/174328005×41168.

Singh, P., et al., 2014. Iron crosslinked alginate as novel nanosorbents for removal of arsenic ions and bacteriological contamination from water. J. Mater. Res. Technol. 3 (3), 195–202. https://doi.org/10.1016/j.jmrt.2014.03.005.

Sosa, A., et al., 2020. Evaluation of the influence of main groundwater ions on arsenic removal by limestones through column experiments. Sci. Total Environ. 727, 138459 https://doi.org/10.1016/j.scitotenv.2020.138459.

Te, B., et al., 2018. Investigation of arsenic removal from water by iron-mixed mesoporous pellet in a continuous fixed-bed column. Water Air Soil Pollut. 229 (9), 296. https://doi.org/10.1007/s11270-018-3935-6.

Thomas, H.C., 1944. Heterogeneous ion exchange in a flowing system. J. Am. Chem. Soc. 66 (10), 1664–1666. https://doi.org/10.1021/ja01238a017.

Tiwari, K., V., A., Chaudhari, C.V., 2020. Mitigation of toxic arsenic (V) from aqueous solution in fixed-bed column using functionally modified bio-polymer. Inorg. Nano Met. Chem. 1–12. https://doi.org/10.1080/24701556.2020.1808994.

Ungureanu, G., et al., 2017. Biosorption of antimony oxyanions by brown seaweeds: batch and column studies. J. Environ. Chem. Eng. 5 (4), 3463–3471. https://doi.org/10.1016/j.jece.2017.07.005.

Verduzco-Navarro, I.P., et al., 2020. Removal of Cu(II) by fixed-bed columns using Alg-Ch and Alg-ChS hydrogel beads: effect of operating conditions on the mass transfer zone. Polymers 12 (10), 2345.

World Health Organization, 2011. Guidelines for drinking-water quality 2011, World Health Organization, Geneva.

Yan, G., Viraraghavan, T., Chen, M., 2001. A new model for heavy metal removal in a biosorption column. Adsorpt. Sci. Technol. 19 (1), 25–43. https://doi.org/10.1260/0263617011493953.

Yin, H., et al., 2017. Removal of arsenic from water by porous charred granulated attapulgite-supported hydrated iron oxide in bath and column modes. J. Clean. Prod. 166, 88–97. https://doi.org/10.1016/j.jclepro.2017.08.026.

Yoon, Y.H., Nelson, J.H., 1984. Application of gas adsorption kinetics. I. A theoretical model for respirator cartridge service life. Am. Ind. Hyg. Assoc. J. 45 (8), 509–516. https://doi.org/10.1080/15298668491400197.